Catalysis Today 387 (2022) 107–118

Contents lists available at ScienceDirect

Catalysis Today

journal homepage: www.elsevier.com/locate/cattod

H_2 production by methane steam reforming over Rh/Al_2O_3 catalyst packed in Cu foams: A strategy for the kinetic investigation in concentrated conditions

Matteo Ambrosetti [1], Danilo Bonincontro [1], Riccardo Balzarotti, Alessandra Beretta, Gianpiero Groppi, Enrico Tronconi *

Politecnico di Milano, Dipartimento di Energia, Via Lambruschini 4, 20156, Milano, Italy

ARTICLE INFO

Keywords:
Methane steam reforming kinetics
Hydrogen
Rhodium catalyst
Process intensification
Open-cell foams

ABSTRACT

The concept of Rh/Al_2O_3 catalyst pellets packed in highly conductive copper foams has been successfully tested in methane steam reforming showing the beneficial effects of thermal conductivity on the obtainment of gradient-less radial temperature profiles. In this work, the same concept is proposed as a strategy for the lab-scale kinetic investigation under concentrated conditions at ambient pressure; thanks to the homogeneous heating of the catalyst mass across the reactor section and the measurement of axial temperature profiles, well-controlled temperature conditions are obtained, and the experimental investigation can be extended to usually unfeasible conditions of high reactant concentrations, overcoming the typical challenges for the kinetic study. Here, steam reforming experiments were performed with CH_4 and H_2O feed molar fractions in the ranges of 10–20 % and 40–90 %, respectively. The co-feed of CO and H_2 was also investigated. A kinetic scheme was developed that substantially confirmed the main results of previous kinetic investigations in annular micro-reactor, performed under diluted conditions; in particular, the first order dependence of the rate of steam reforming on methane partial pressure, the independence from H_2O partial pressure, and the important inhibiting effect of CO were confirmed. The independence of the reaction rate from the H_2 co-feed was here demonstrated for the first time. The new experimental campaign allowed to identify more clearly the kinetic dependencies of the water gas shift reaction, positively influenced by H_2O partial pressure but scarcely affected by CO partial pressure, which could be also explained based on the inhibiting effect of surface CO coverage. Parameter estimates were obtained by model fit over a wide temperature range (400–850 °C), conveying robustness to the proposed kinetic scheme for future reactor design applications.

1. Introduction

In the history of Industrial Chemistry, Hydrogen has represented one of the most important chemicals. According to International Energy Agency [1], chemical and petrochemical applications account for more than 95 % of pure hydrogen and 70 % of the total hydrogen demand, the majority of which is used for ammonia production, methanol production and refining processes. These are characterized by an economy of scale and therefore require large and centralized H_2 plants [2,3].

Methane Steam Reforming (MSR) is the most used H_2 production technology. The process involves both methane reforming with steam and water gas shift:

$$\text{MSR} \quad CH_4 + H_2O \rightarrow CO + 3\,H_2 \quad \Delta H\,(298\ K) = +206\ kJ/mol \tag{1}$$

$$\text{WGS} \quad CO + H_2O \rightarrow CO_2 + H_2 \quad \Delta H\,(298\ K) = -41.1\ kJ/mol \tag{2}$$

The endothermic character of the MSR reaction calls for efficient heat supply at high reaction temperatures, which is obtained by the multi-tubular design of the reformer, where slender catalyst-packed tubes are externally heated by burners and flue gases. To promote the radial heat transfer in the tubes (the limiting step of the process), high flow velocities are required, and 10–12 m long tubes are needed to reach almost complete CH_4 conversion [3]. The reactor is operated at high pressures, as required by the end-users. Industrial catalysts for methane steam reforming are typically based on $Ni/MgAl_2O_4$

* Corresponding author.
E-mail address: enrico.tronconi@polimi.it (E. Tronconi).
[1] These authors contributed equally to this work.

https://doi.org/10.1016/j.cattod.2021.06.003
Received 5 March 2021; Received in revised form 25 May 2021; Accepted 3 June 2021
Available online 6 June 2021

formulations that provide an optimal tradeoff between cost, activity and long term stability under the severe operating conditions [4–6].

Optimized at the large scale, the MSR technology is little flexible to scaling down. However, the growing penetration of low-carbon hydrogen uses as clean energy vector calls for the development of a distributed network of H_2 production. New hydrogen applications include transportation, industrial and residential heating and Combined Heat and Power (CHP) generation [7,8]. In the transition to a fully green and decarbonized H_2-production capacity, small-scale fuel processors can represent the key for supporting in the short term the H_2 demand of the energy market. Despite decades of experience in the design of large-scale steam reforming units, two main factors challenge the intensification of MSR: (i) the high endothermicity of the reaction and (ii) the need of suitable catalysts able to grant high yields of H_2 also at intermediate temperatures.

In order to mitigate problems associated to heat transfer at the small scale, several kinds of structured reactors have been proposed for the intensification of energy-demanding catalytic processes [9]. One of the possible approaches is the coupling at the micro-scale of endothermic and exothermic reactions with coated micro-channel reactors to promote the heat exchange between the two processes [10–12]. The application of conductive internals has been proposed as a solution to reduce the thermal gradients inside the reactors and improve the process productivity; in early studies, stainless steel structures were proposed in steam reforming applications thanks to their tolerance to high temperatures [13–15]. However, the nature and geometry of the metal support and the resulting effective thermal conductivity need to be optimized for the single process to obtain the desired beneficial effect. The heat transfer properties of different structured catalysts (i.e, open-cell foams, monoliths and more recently periodic open cellular structures – POCS) have been investigated in our group [16–18] and showed the potential of these structures. Open-cell foams are interconnected solid structures composed by a solid matrix characterized by ligaments that create interconnected cells communicating through windows. Thanks to this feature, open-cell foams enable high effective heat transfer properties through the conduction in the solid metal. The small cell size enable high surface area and increase the wall heat transfer coefficient [19].For the catalytic applications, both washcoating with thin active layers [12,20] or packing with small catalytic pellets [21] were proposed as feasible strategies. In the case of methane steam reforming the use of Cu-foams either washcoated or packed with Rh/Al_2O_3 catalyst particles has been proved to be highly promising for the process intensification [20, 21]. In particular, in [21] the outstanding performances of packed copper open-cell foams were demonstrated. On one side, packing allows for a reasonably high catalyst inventory if small pellets are adopted, on the other side remarkably high heat transfer properties are realized by the synergy between the packing and the conductive internals. Besides, the use of a Rh based formulation guarantees high intrinsic activity in a wide temperature range and low coking tendency [22].

In this work, the same reactor concept has been applied to a more fundamental objective, that is the extension of the kinetic investigation of methane steam reforming on Rh to concentrated H_2O/CH_4 feeds at ambient pressure. As well known, the kinetic study of fast and highly exothermic or endothermic reactions is challenged by irreducible mass and heat transport resistances [23]. Traditional packed-bed reactors suffer from the onset of important radial and axial temperature profiles that hinder a rigorous kinetic investigation [24]. Use of fine particles, dilution of the catalyst bed and/or of the reactant mixtures are common strategies of mitigation of the thermal and diffusional effects. Iglesia and co-workers obtained a gradient-less reactor configuration by introducing a very large degree of dilution both at the scale of the particle and at the scale of the bed [25]; diluted feed streams were used as well. The "infinitely" diluted reactor design was applied to a very wide and systematic investigation of the kinetic regimes of CH_4 activation with O_2, H_2O and CO_2 over noble metal catalysts, including Rh, Pt and Pd [25, 26]. In the case of Rh-catalyst, the rate of CH_4 steam reforming was found proportional to the partial pressure of CH_4 and independent from the concentration of H_2O and reaction products, an indication of the unique kinetic relevance of the first C–H bond cleavage. Water gas shift was found to be fully equilibrated. Due to the high level of bed dilution, the experiments could be reliably evaluated only within the differential conversion regime, which is an important limitation in the perspective of reactor design applications.

Integral data were instead collected in our laboratory by using an annular reactor, especially designed for running kinetic tests of fast catalytic reactions, at high space velocity and under controlled temperature conditions [27,28]. The reactor consists of an annular duct, which is obtained by introducing a catalyst coated ceramic capillary into a quartz tube; because of a very efficient heat radiation mechanism from the catalyst surface, partial oxidation, steam reforming and CO_2-reforming experiments could be performed under quasi-isothermal conditions. In fact, the axial temperature profile was characterized by very limited gradients (few degrees over the catalyst layer length) under diluted conditions (1–4 % v/v CH_4 concentration). By means of reactor modelling (including the impact of inter-phase mass transfer limitations), the kinetics of methane, CO and H_2 fuel rich oxidations, as well as the kinetics of methane steam reforming and water gas shift over Rh/Al_2O_3 were obtained. Similarly to Iglesia and coworkers' studies [25,29], the rate of steam reforming was found proportional to the methane concentration and unaffected by H_2O concentration; however, the data collected in integral regime evidenced an overall reaction order lower than one, which ascribed to the inhibiting effect of products adsorption. Besides, water gas shift was non-equilibrated below 500 °C. Partial oxidation experiments were also performed under concentrated feed streams (27 % v/v CH_4), at the expense of pronounced but measurable axial temperature gradients. These concentrated tests were used to verify the adequacy of the C1 kinetic model. Additional pieces of evidence on the prevailing kinetic dependences and the evolution of surface coverages were provided by a micro-kinetic study, incorporating DFT estimates of the enegetics [30].

The kinetic investigation has been extended to the partial oxidation and steam reforming of several other hydrocarbon fuels [31,32]; throughout the studies, the kinetics of the water gas shift has been further refined [22] with the proposal of a main kinetic dependence on H_2O partial pressure. Notably, in all these experimental campaigns, the total C concentration has been limited on purpose to 3% (molar) in order to minimize temperature gradients along the axial coordinate and the radial gradients across the gas and solid phases.

To overcome such limitations, an entirely new strategy was needed. Thanks to the superior heat and mass transfer properties granted by the presence of the conductive reactor internals based on open-cell foams, the Rh/Al_2O_3 formulation was herein tested in methane steam reforming under considerably larger concentration of reactants, while spanning throughout the entire integral regime from low to high conversions. The new experimental campaign has offered the opportunity to verify in a more stringent way the kinetics of methane steam reforming and water gas shift previously proposed and thus develop a more robust kinetic model.

2. Materials and methods

2.1. Catalyst preparation and characterization

The catalyst used in this work is the same already used in previous investigations of the group [18,19]. Catalytic tests were performed using a home-made Rh/Al_2O_3 catalyst in the form of egg-shell particles to avoid the presence of internal mass transport limitations. Alumina particles (Puralox by Sasol, 600 μm nominal diameter, d50 = 660 μm) were preliminary dried in a static oven at 120 °C overnight; then, Rh was deposited by wet impregnation by diluting Rh $(NO_3)_3$ liquid solution (12.5 %wt. metal content by Alfa Aesar) with deionized water. The amount of solution was calculated with an excess of 25 % with respect to

the pellet pore volume saturation, while the solution concentration was calibrated to reach a Rh content per mass of pellet equal to 0.3 wt %.

The catalytic material was characterized in a previous work [21] with a scanning electron microscope (ZeissEvo50 EP) equipped with an energy dispersive X-ray spectrometer (EDX) to determine the concentration profile of rhodium in the radial direction of cross-sectioned catalytic pellets.

The total metal content, in terms of Rh° with respect to the Al_2O_3 matrix, was found to be equal to 0.28 %wt. with respect to Al_2O_3 support mass, which is in good accordance with the specification (0.3 %wt.) The dispersion of Rh was previously quantified equal to 90 % by H_2 chemisorption.

The thickness of the egg-shell layer was found to be 38 ± 2 μm, which is consistent with results reported in literature for catalysts produced with a similar preparation procedure [21,33]. A posteriori analysis of internal mass transport limitations was performed with the kinetic model derived from the experimental tests by calculating the local effectiveness factor.

2.2. Experimental setup

Catalytic tests have been carried out in a lab scale reactor inserted in a controlled temperature furnace (Carbolite GERO 30–3000 EVZ 1200, Fig. S2 e). The reactor is an AISI 310S stainless steel tube, 68 cm long and with an internal diameter of 2.95 cm and external diameter of 34 mm. Packed foam catalytic bed (7.5 cm) was prepared using as internals six 40 PPI (pores per inch) copper foams segments (ERG Duocell, cell diameter (d_{cell}) =2 mm, void fraction $\varepsilon_f = 0.89$). The foams were kept in the desired position (40 cm from the bottom of the reactor) by a spacer composed by a 40 PPI FeCrAl foam soldered with the two internal thermowells (see Fig. S1 in SI). A FeCrAl felt was used to separate the FeCrAl foam and the copper ones to retain catalytic bed particles. The latter were loaded as described in Balzarotti et al. [21] by gentle pouring from the top in order to fill the foam cavities. In order to improve packing efficiency, the reactor was gently shaken during the catalyst loading. This combination of pellet and foams allows a good packing, thus avoiding gas bypass and void regions in the catalytic bed as previously reported [34]. Thus, the foams have been filled with 3.93 g of Rh/Al_2O_3 pellets and 26.17 g of bare Al_2O_3 pellets, with a resulting void fraction of the packed foam ($\varepsilon_{PF} = 1\text{-}V_{pellet}/(V_F{}^*\varepsilon_f)$) of 0.48, in line with previous results. A porosity lower than 0.55 can be considered as a safe value to exclude the presence of bypass in the reactor that may influence catalytic measures [34]. On top of catalytic bed, 3 cm of inert Al_2O_3 pellets (d_{pellet} =1.6 mm Puralox by Sasol) have been loaded to allow full mixing of the reactants.

Reaction mixture has been fed downward from the reactor top. CH_4, CO, H_2, N_2 (SAPIO, purity 99.999 %) have been fed through separate lines and their flow rates has been controlled by dedicated flowmeters (Brooks SLA5800 Series, Figs. S2b in SI). Water vapor was fed to the reactor, first feeding a calibrated amount of liquid water (stored in two vessels, Figs. S2a in SI) through a flowmeter (Brooks IP40 QUANTIM Series, Figs. S2c, in SI) followed by an evaporator (Brooks VDM300, Figs. S2d in SI). All the lines between evaporator and reactor have been heated and insulated to prevent water condensation. The system was operated at ambient pressure. At the reactor bottom, a condenser allows the recovery of the unreacted water (Figs. S2f in SI), while incondensable gases are sent to the GC (GCX, Pollution SRL, Figs. S2g in SI) equipped with MolSieve and Porapack columns connected to TCD detectors for their online quantification. A calibrated stream of N_2 was mixed after the condenser with the reaction products in order to allow the quantification with internal standard method. Water was calculated according to methane consumption and CO_2 production and stoichiometries of reactions (1) and (2). The overall absolute errors detected in carbon balances were in the range of 1–5%.

Temperature has been monitored with three sliding thermocouples inserted in stainless steel thermowells (O.D: =3.2 mm), having the same configuration as described in Balzarotti et al. [21] In particular, one of them was placed at the centerline of the foam (Center-T, figure), a second one was placed at r = R/2 (Radial-T) and the third one was placed outside the reactor (Wall-T), solidly soldered to the reactor wall. In this way, it has been possible to measure the temperature profiles during the tests by sliding the thermocouples with a sampling resolution in the axial direction equal to 5 mm, along 12.5 cm. As shown in Fig. 1c, axial coordinate has been defined in order to have the origin of this length 2.5 cm before the catalytic bed.

As far as the operative conditions of the catalytic tests are concerned, the oven temperature has been modulated within the 400−750 °C range, while three different Gas Hourly Space Velocities (GHSV) have been tested: 32900, 65700 and 98600 N L h^{-1} kg_{cat}^{-1}. In terms of reaction mixture compositions, different H_2O/CH_4 (S/C) ratios have been employed to investigate the effect of composition on the reaction kinetics. In particular, the first experiments have been carried out modifying the CH_4 and H_2O molar fraction between 9.75–19.50 % and 40.25–90.25 %, respectively, and using N_2 as complement, corresponding to a molar steam to carbon ratio (S/C) in the range 4.1 – 8.3. A second group of tests aimed at evaluating the effect of products cofeeding and was performed by introducing precise amount of CO and H_2 to the feed.

Catalytic tests at fixed operative conditions (GHSV = 65700 N L h^{-1} kg_{cat}^{-1} T_{oven} = 500 °C, S/C = 4.1 CH_4 = 19.5 %) to evaluate catalyst stability have been carried out after each experimental run.

3. Results

3.1. Characterization of the thermal behavior of the system at varying load: effects of heating temperature and total flow rate

Catalytic tests were carried out to fully characterize the thermal performances of the system (i.e., axial and radial temperature profiles) at varying heating temperature and integral CH_4 conversion, that is at varying total thermal load; in practice, experiments were performed by increasing the oven temperature from 450 to 700 °C and the total flow rate from 2 to 6 Nl/min. The experiments were performed at the constant S/C ratio of 4.1, in non-diluted conditions (CH_4 feed molar fraction of 19.5 %). The results are reported in Fig. 2, in terms of measured conversion vs heating temperature (panel a) and vs. a representative reactor temperature (panel 2b), at three levels of space velocity.

At the smallest GHSV of 32900 N L h^{-1} kg_{cat}^{-1} and increasing heating temperature, the measured CH_4 conversion grew from about 10 % to about 95 %. At each heating temperature, then, lower conversions were progressively measured at increasing space velocity, a clear indication of the kinetic sensitivity of the system (Fig. 2a). At the highest space velocity of 98600 N L h^{-1} kg_{cat}^{-1}, the measured conversion grew from 5 to 75 % at increasing heating temperature. Thus, in the entire experimental campaign, the reactor experienced an overall change of the thermal load by a factor of over 20.

In each experiment, the axial temperature profile at the three radial coordinates was measured, thus monitoring the whole temperature distribution across the reactor volume.

Fig. 3 reports the measured profiles for selected representative conditions, namely for three values of space velocity at the two oven temperatures of 500 and 700 °C. All the experiments were characterized by the presence of a cold spot, where the bed temperature is lower than the oven temperature. The extent of the cold spot was affected by both the GHSV and the oven temperature and it increased its magnitude at increasing total load (that is converted CH_4 molar flow) of the experiment. However, the axial temperature profiles recorded in the central and mid-radius positions were almost superimposed in all the tests, while a significant difference with the wall temperature was present. This is consistent with the experimental observations and the theoretical evaluations performed in previous studies, where we addressed the quantitative characterization of heat transfer in conductive packed

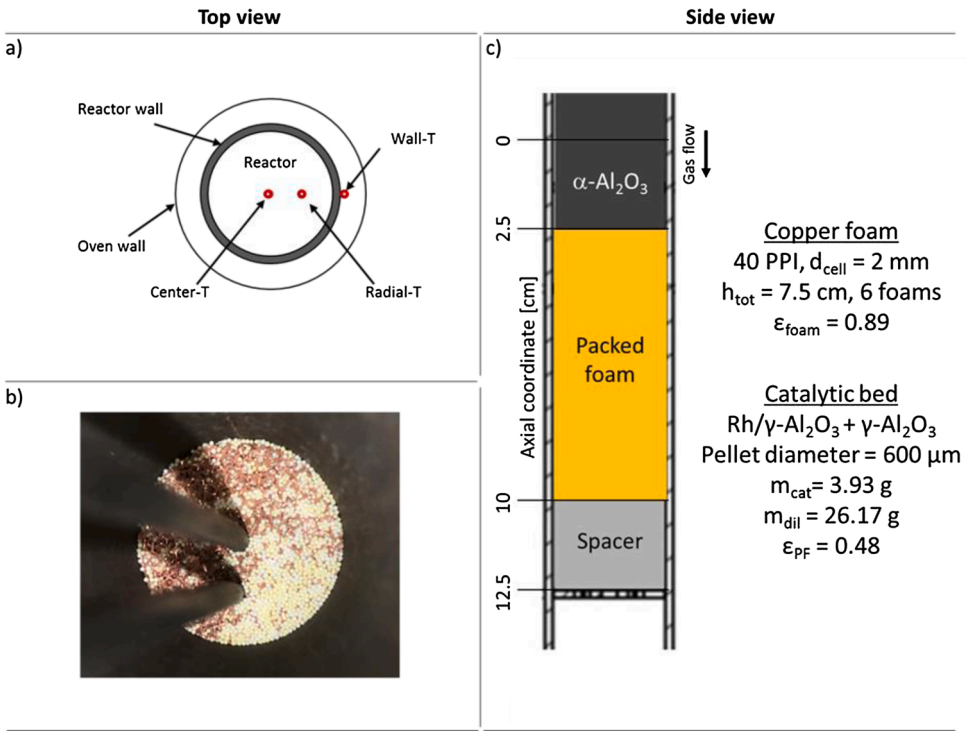

Fig. 1. (a) Top view graphical representation of the reactor layout with the three thermocouples; (b) top view of packed foam; (c) side view of the reactor layout.

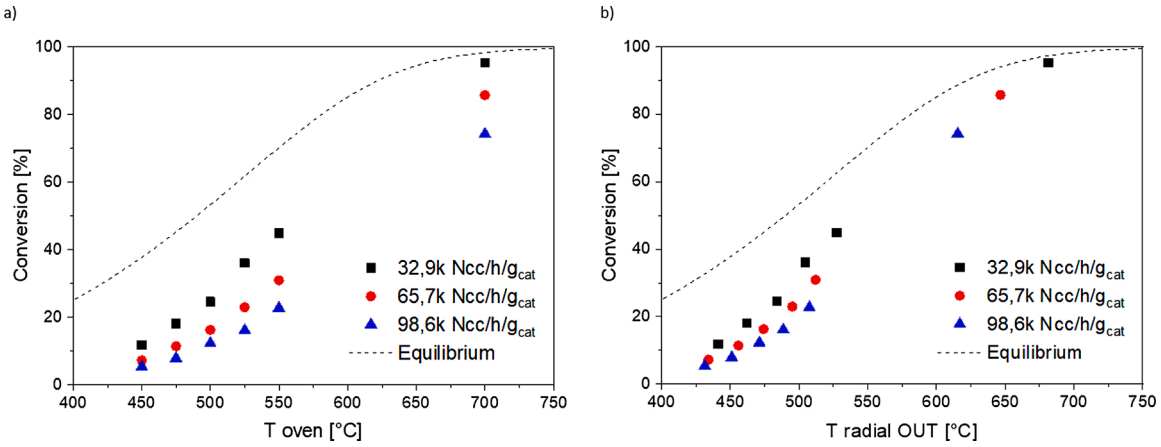

Fig. 2. CH_4 conversion as a function of oven temperature (a, left) and outlet temperature in radial position (b, right). Operative conditions: S/C ratio 4.1; GHSV: 32900, 65700 and 98600 N L h^{-1} kg_{cat}^{-1} (black square, red circle and blue triangle, respectively). Dotted line: equilibrium CH_4 conversion. (For interpretation of the references to colour in this figure legend, the reader is referred to the web version of this article.)

foams [21]; there, we concluded that the same reactor design herein tested is characterized by very high axial and radial effective conductivity (in excess of 20 W/m/K) [18] and a concentrated heat transfer resistance at the wall (that is at the interface between the foam peripheral surface and the inner reactor tube wall). In fact, by using a lumped heat transfer model developed in [21] it was found that the overall heat transfer coefficients of packed open-cell foams are in the range of [400–700] W/m^2/K : the wall heat transfer resistance is responsible for over 85 % of the overall resistance. Based on these considerations, we believe legitimate to assume that across the section of the foam at each axial coordinate the temperature was essentially constant.

The analysis of the temperature profiles suggests that at increasing flow rate the observed decline of conversion resulted from the combined effects of contact time and of temperature reduction. Thus, a more "kinetically" informative representation of the conversion measurements is the one proposed in Fig. 2b, where data are plotted against the measured outlet temperature at the mid-radius coordinate. The selection of an outlet temperature rather than an average bed temperature allows for a more rigorous comparison with the chemical equilibrium curve, which has been calculated by the extent of reaction method using the methane steam reforming (1) and the water gas shift (2) independent stoichiometries with DG° temperature functions taken from literature [35]. The same standard of data representation was adopted throughout the kinetic study, thus making easier the qualitative evaluation of the impact of thermodynamic constraints on the observed conversions and product distributions. The representation of Fig. 2b further emphasizes that, in the ranges of space velocity herein explored, the reactor operated mainly under a kinetically controlled regime below 600 °C (where the effect of space velocity was found), but approach to equilibrium influenced the high temperature behavior. On the bases of this evidence the kinetic tests described in the next section have been

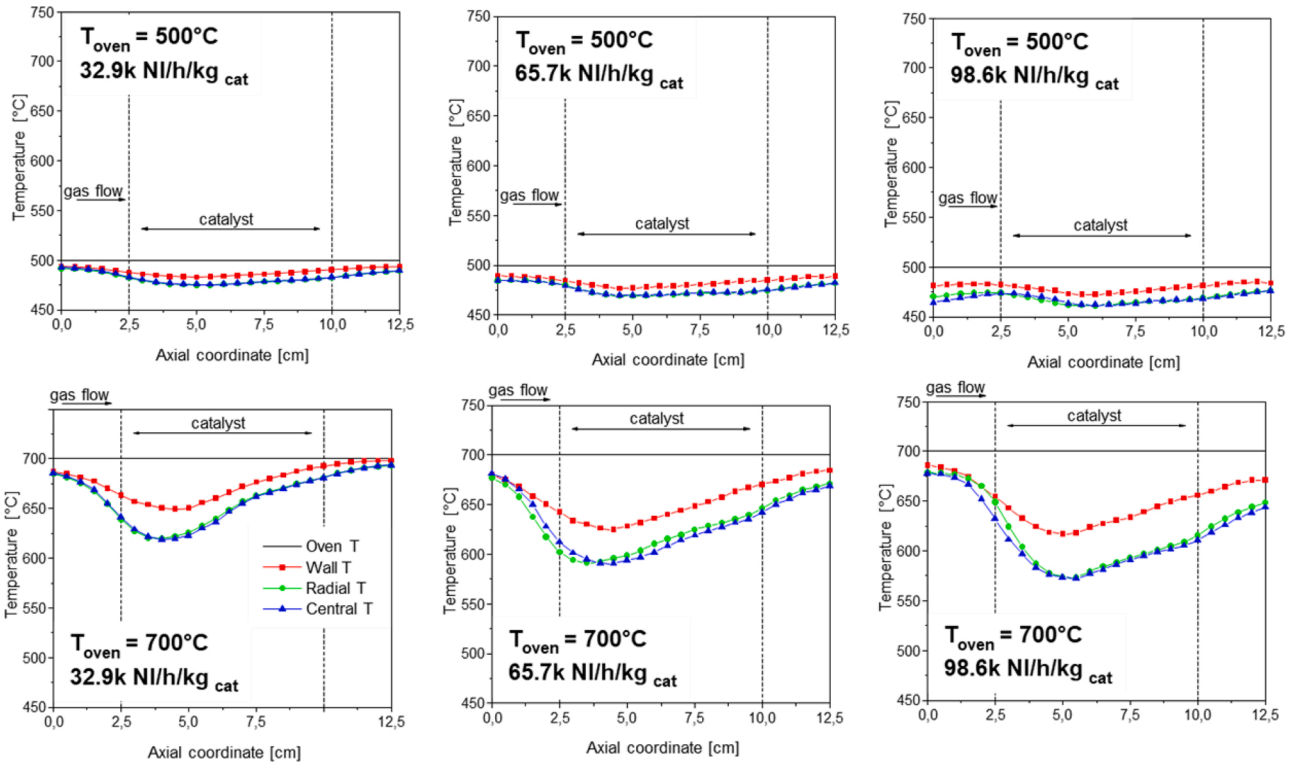

Fig. 3. temperature profiles for the different GHSV and T_{oven} of 500 and 700 °C (top and bottom, respectively). Solid line: oven set temperature; symbols with lines: experimental temperature measurements at the bed at centerline (blue triangles), r/2 (green circles) and external wall temperature (red squares); dashed vertical lines: position of the catalytic bed. (For interpretation of the references to colour in this figure legend, the reader is referred to the web version of this article.)

performed at GHSV = 65700 N L h^{-1} kg_{cat}^{-1}

3.2. Kinetic analysis - experimental results

After proving the heat transfer efficiency granted by the presence of the copper foams and identifying proper operating conditions that enable to investigate the chemical process far from the equilibrium, the effects of variation of partial pressure of reactant and products were investigated. First, the effects of CH_4 and H_2O partial pressures were investigated in the ranges 9.75–19.50 % v/v and 40.25–90.25 % v/v, respectively. In all the tests the H_2O/CH_4 feed ratio was kept higher than 4 to avoid coke formation. Inert N_2 was fed to balance. Then, the effects of co-feed of CO and H_2 were investigated. In each run, 7 different oven temperatures in the range 450–750 °C were tested. Overall, 10 different runs (see Table S1 in SI) and 70 tests were performed. CH_4 conversion in Reference tests periodically repeated to verify the catalyst stability are reported in the supplementary information (see image S5).

The results of the runs performed at varying CH_4 feed concentration are plotted in Fig. 4 as a function of the bed outlet temperature measured at the mid-radius position.

It can be observed that the increase of CH_4 concentration led to a decrease of conversion, suggesting an apparent global reaction order of MSR less than 1. This effect is evident at temperatures below 650 °C, whereas at higher temperatures the conversion data were close to 100 %, aligned with the equilibrium. On the other hand, at the lowest temperatures investigated, the production of H_2, CO and CO_2 was little affected; at increasing temperature, a positive effect of the reactant concentration became more important. At the highest temperatures, the concentration of products was bound by the stoichiometric and thermodynamic limits. It may be concluded that the process showed an apparent reaction order in the range 0–1, growing with increasing temperature.

Interestingly, up to 550 °C, the main reaction products were CO_2 and H_2, which suggests a very efficient displacement of CO, produced by methane steam reforming, into CO_2 by water gas shift. In the same temperature range (i.e., far from the equilibrium conditions), the productivity of CO_2 was mainly dependent on temperature but negligibly affected by the varying feed CH_4 concentration, which suggests an overall apparent order on CO close to zero. At higher temperatures, the composition of the syngas closely approached the thermodynamic equilibrium and was characterized by the growing concentration of CO, the flattening of H_2 concentration and a mild negative trend of CO_2 concentration with increasing temperature.

The effect of water at fixed methane concentration is then shown in Fig. 5.

The measured CH_4 conversion was positively affected by the increase of water concentration, and an increase of productivity of H_2 and CO_2 was observed. Instead, the outlet molar fraction of CO decreased progressively at increasing water concentration; within the kinetically relevant temperature-range, this was a clear evidence of the consecutive nature of water gas shift and of its positive kinetic dependence on the concentration of water.

Additional experiments were performed by enriching the methane/steam feed with CO and H_2. Two runs were carried out with 4.9 and 7.6 % CO co-feed and the results are reported in Fig. 6. The addition of CO caused an appreciable drop of CH_4 conversion at the lowest temperatures, where kinetic effects prevailed.

At 7.6 % CO co-feed, the negative effect was so important that at 450 °C heating temperature the conversion of methane was almost negligible, and the test assumed the form of a water gas shift experiment, where about 50 % of the fed CO was converted into CO_2. Indeed, the outlet concentration of CO passed through a minimum at increasing temperature, which clearly resulted from the combination of CO consumption by WGS and hindered CO production by MSR.

This evidence corroborated the hypothesis that CO plays an important inhibiting role in the kinetics of the MSR reaction on Rh. Such inhibiting effect had been already observed in our laboratory under more diluted conditions [28,36] and by other research groups [37], who

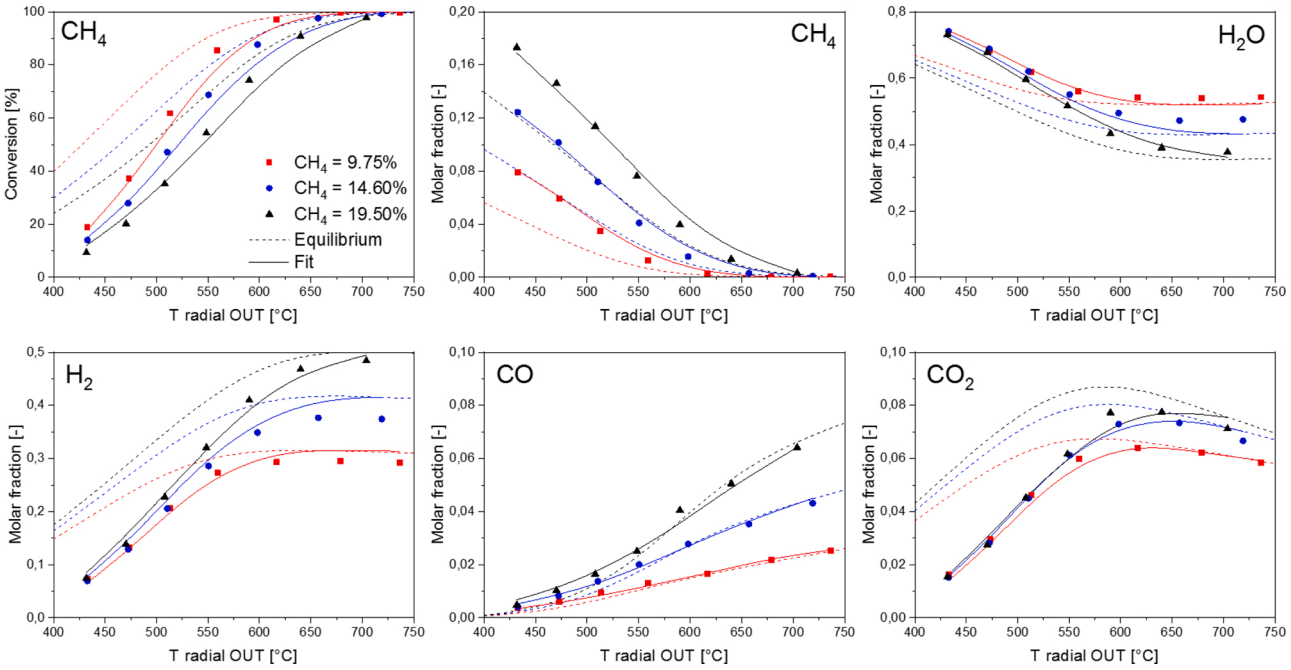

Fig. 4. Effect of CH_4 feed concentration on: (top from left) CH_4 conversion, outlet CH_4 concentration, outlet H_2O concentration, (bottom from left) outlet H_2 concentration, outlet CO concentration, outlet CO_2 concentration). Symbols: experimental measurements, dotted lines: thermodynamic equilibrium, continuous lines: model fit. Operative conditions: GHSV 65700 N L h^{-1} kg_{cat}^{-1}; H_2O volume fraction 80.50 %; CH_4 volume fractions 9.75, 14.60 and 19.50 % (red, blue and black, respectively); N_2 volume fractions 0, 4.90 and 9.75 % (red, blue and black, respectively). (For interpretation of the references to colour in this figure legend, the reader is referred to the web version of this article.)

suggested that CO is the most abundant specie adsorbed on the catalyst under the investigated conditions.

On the other hand, by looking at CO_2 concentration, it is evident that WGS activity was enhanced by increasing CO concentration from the bed entrance, suggesting a positive reaction order of WGS with respect to CO.

Interestingly, the outlet H_2 molar fraction responded to the combined effects of CO-cofeed on MSR and WGS; in fact, it decreased with increasing CO co-feed at temperatures below 600 °C, due to the hindering effect on MSR, but it increased with increasing CO content at the

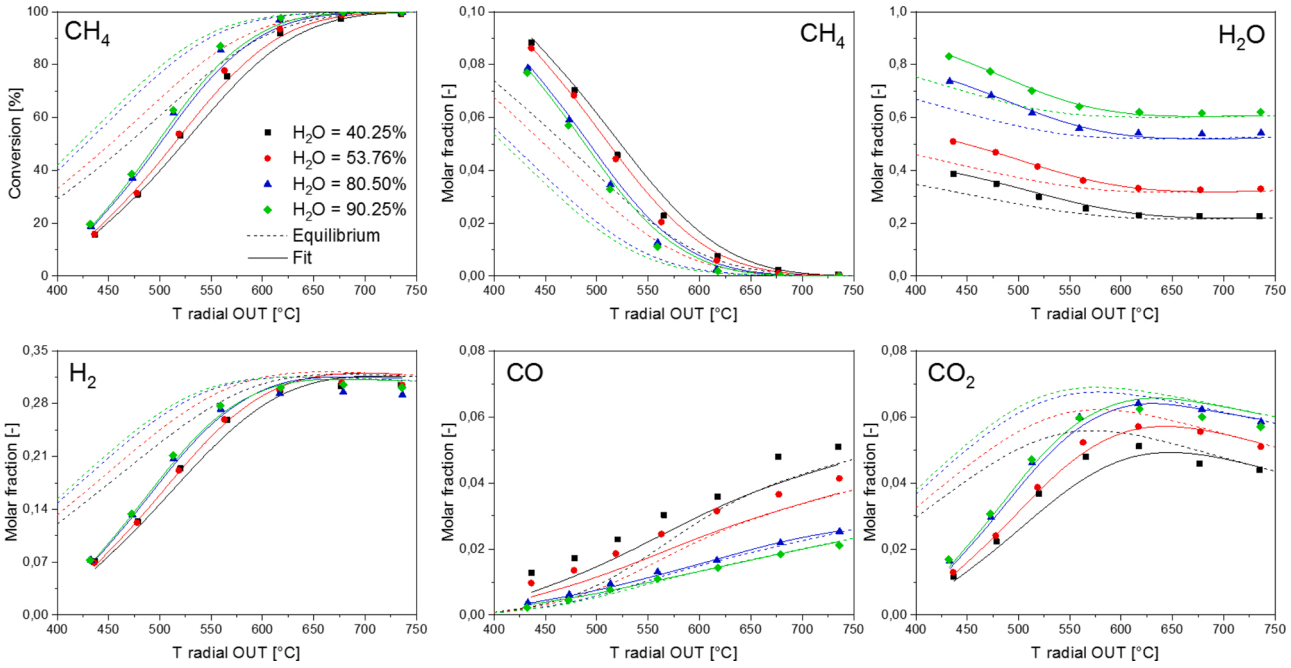

Fig. 5. Effect of H_2O feed concentration on: (top from left) CH_4 conversion, outlet CH_4 concentration, outlet H_2O concentration, (bottom from left) outlet H_2 concentration, outlet CO concentration, outlet CO_2 concentration). Symbols: experimental measurements, dotted lines: thermodynamic equilibrium, continuous lines: fitted values. Operative conditions: GHSV 65700 N L h^{-1} kg_{cat}^{-1}; CH_4 volume fraction 9.75 %; H_2O volume fractions 40.25, 53.76, 80.50 and 90.25 % (black, red, blue and green, respectively); N_2 volume fractions 50.00, 36.49, 9.75 and 0% (black, red, blue and green, respectively). (For interpretation of the references to colour in this figure legend, the reader is referred to the web version of this article.)

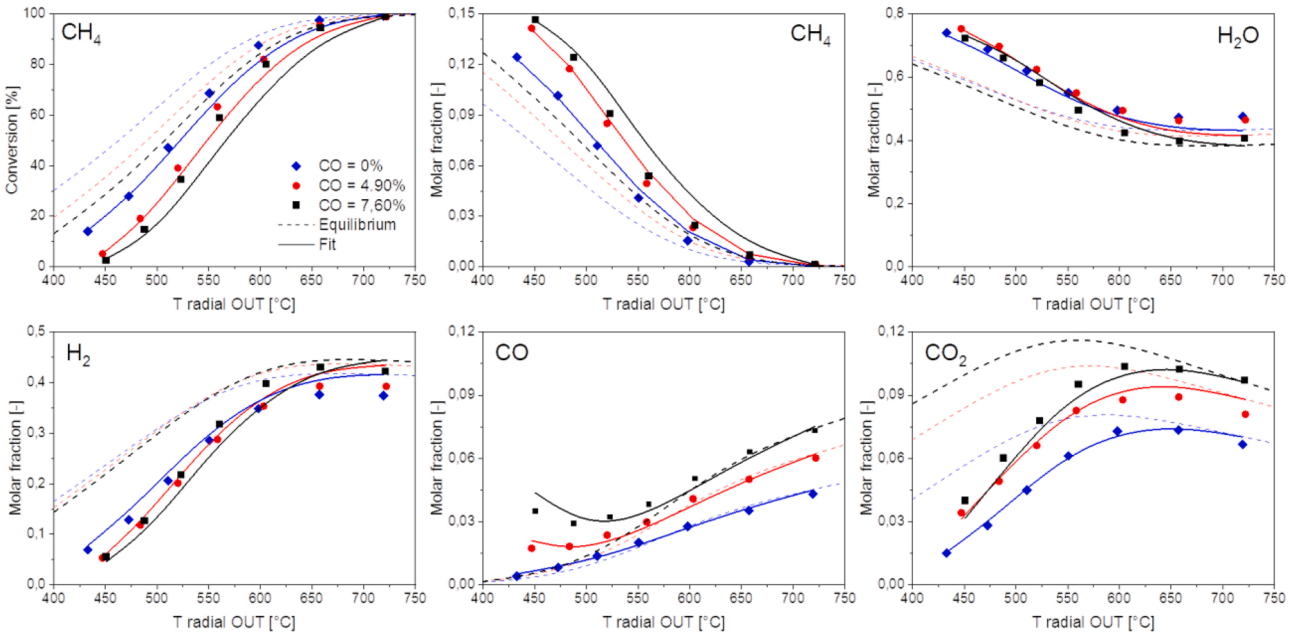

Fig. 6. Effect of CO feed concentration: (top from left) CH_4 conversion, outlet CH_4 concentration, outlet H_2O concentration, (bottom from left) outlet H_2 concentration, outlet CO concentration, outlet CO_2 concentration). Symbols: experimental measurements, dotted lines: thermodynamic equilibrium, continuous lines: fitted values. Operative conditions: GHSV 65700 N L h^{-1} kg_{cat}^{-1}; CH_4 volume fraction 14.60 %; H_2O volume fractions 80.50 %; N_2 volume fractions 4.90 and 0% (blue and red, respectively); CO volume fractions 0 and 4.90 % (blue and red, respectively). (For interpretation of the references to colour in this figure legend, the reader is referred to the web version of this article.)

highest temperatures, in line with the equilibrium of WGS.

An additional experiment was performed with 9.75 % H_2 co-feed (run 9 in Table S1) and the results are compared in Fig. 7 and with those of run 10 w/o H_2 in the feed, which was performed just after the H_2 co-feed one, to remove the effect of moderate deactivation which was observed during the repeated standard tests (see last points in Figs. S5 of SI).

No appreciable effect was observed on conversion and product distribution, indicating that the kinetics of MSR and WGS were not influenced by the H_2 concentration. Since the catalyst was in part deactivated and no effect of H_2 was found, these tests were not included in the regression.

In conclusion, the experimental campaign revealed the following qualitative dependences.

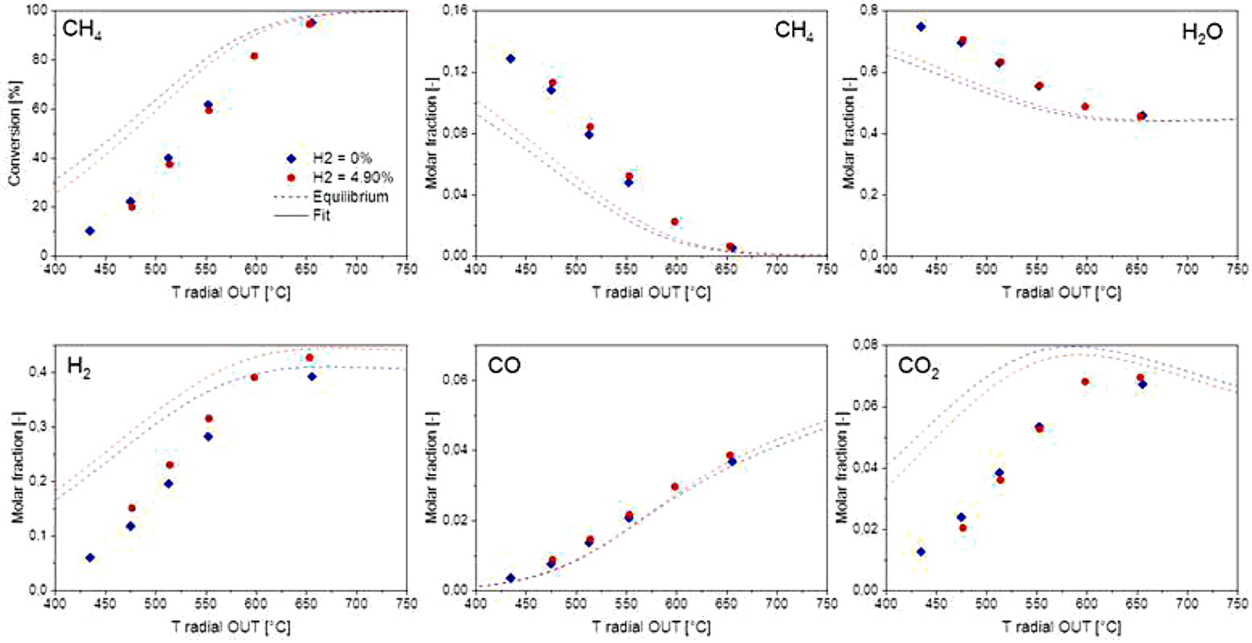

Fig. 7. Effect of H_2 feed concentration: (top from left) CH_4 conversion, outlet CH_4 concentration, outlet H_2O concentration, (bottom from left) outlet H_2 concentration, outlet CO concentration, outlet CO_2 concentration). Symbols: experimental measurements, dotted lines: thermodynamic equilibrium. Operative conditions: GHSV 65700 N L h^{-1} kg_{cat}^{-1}; CH_4 volume fraction 9.75 %; H_2O volume fractions 80.50 %; N_2 / H2 volume fractions 4.90 and 0% (blue and red, respectively); H_2 volume fractions 0 and 9.75 % (blue and red, respectively). (For interpretation of the references to colour in this figure legend, the reader is referred to the web version of this article.)

Concerning MSR, data gave evidence of:

- a reaction order with respect to CH_4 in between 0 and 1, growing with temperature;
- an apparent positive order of water;
- an apparent negative order of CO;
- a zeroth order dependence on H_2.

Concerning WGS, data gave evidence of:

- an apparent positive order of CO
- an apparent positive order of H_2O
- a zeroth order dependence on H_2

3.3. Kinetic analysis: data fitting

The kinetic analysis of experimental data was performed by assuming (i) a kinetic scheme consisting of the two independent reactions (1) and (2), and (ii) a PFR pseudo-homogeneous non-isothermal model. The model includes the differential mass balances for the reacting species:

$$\frac{dF_i}{dW_{cat}} = \sum_j \nu_{i,j} r_j \mathrm{i} = \mathrm{CH4,\ H2O,\ H2,\ CO,\ CO2} \tag{3}$$

Differential mass balances were solved using the routine *fsolve* in Matlab.

The axial temperature profiles have been assigned by fitting the experimental temperature measurements of the lateral thermocouple with a 5th order polynomial (see Figs. S4 in SI), whereas radial temperature differences have been neglected in line with the results reported in section 3.1.

Based on the qualitative evidence reported above, the following rate expressions were assumed for the two reactions (1) and (2):

$$r_{MSR} = \frac{k_{MSR}\, P_{CH_4} \left(1 - K_{P,MSR}/K_{EQ,MSR}\right)}{1 + K_{ads_{CO}}\, P_{CO}} \left[\frac{mol}{gcat\ s}\right] \tag{4}$$

$$r_{WGS} = \frac{k_{WGS}\, P_{H_2O}\, P_{CO}}{1 + K_{ads_{CO}}\, P_{CO}} \left(1 - K_{P,WGS}/K_{EQ,WGS}\right) \left[\frac{mol}{gcat\ s}\right] \tag{5}$$

Rate expression (4) reproduces the same expression proposed in a previous work [26], based on highly diluted steam reforming data obtained in the isothermal annular reactor; it considers a first order dependence on methane and zeroth order dependence on water in line with the intrinsic turnover rate measurements obtained by Wei and Iglesia on Rh under differential regime [25]. However, it also includes a term at the denominator accounting for the competitive adsorption of CO, whose inhibiting effect was clearly demonstrated by the data obtained in this and previous studies [22,28] under integral regime.

Concerning the water gas shift reaction, it is interesting to observe that in our previous studies in annular reactor and diluted feed streams [22] we had proposed a zeroth order dependence on CO and a first order dependence on water. Based on the evidence herein collected, rate expression (5) was modified to account for a variable order in CO, through the introduction of a linear dependence on CO partial pressure together with a competitive adsorption term. Such an expression is in line with the studies of Deutschmann and coworkers, who identified the reaction between CO and OH as the rate determining step of the WGS over nickel and rhodium sites [38]. The same rate determining step has been identified by Maestri et al. over Rh(111) sites, based on DFT studies [39].

The reversible nature of both MSR and WGS was accounted for by introducing terms of approach to equilibrium:

$$\left(1 - K_{P,MSR}/K_{EQ,MSR}\right) \text{ with } K_{P,MSR} = \frac{P_{CO} P_{H2}^3}{P_{CH4} P_{H2O}} \tag{6}$$

and

$$\left(1 - K_{P,WGS}/K_{EQ,WGS}\right) \text{with } K_{P,WGS} = \frac{P_{CO2} P_{H2}}{P_{CO} P_{H2O}} \tag{7}$$

Kinetic and adsorption constants were re-parametrized as follows to reduce the correlation among parameters:

$$k_j(T)\left[\frac{mol}{atm\ g_{cat}\ s}\right] = k_{0,j}(T_0)\ \exp\left[-\frac{E_{act,j}}{R}\left(\frac{1}{T} - \frac{1}{T_0}\right)\right] \tag{8}$$

$$K_{ads,i}(T)\left[\frac{1}{atm}\right] = K_{ads_0,j}(T_0)\ \exp\left[-\frac{\Delta H_{i,\,ads}}{R}\left(\frac{1}{T} - \frac{1}{T_0}\right)\right] \tag{9}$$

with the reference temperature $T_0 = 873$ K.

The model was adapted to the population of experiments and the kinetic parameters were estimated by minimizing the following objective function:

$$fmin = \sum_i \left(\frac{\lambda_{MSR}^{experimental} - \lambda_{MSR}^{model}}{\lambda_{MSR}^{experimental}}\right)^2 + \left(\frac{\lambda_{WGS}^{experimental} - \lambda_{WGS}^{model}}{\lambda_{WGS}^{experimental}}\right)^2 \tag{10}$$

where λ_{MSR} and λ_{WGS} are the extents of MSR and WGS, calculated from the net molar flow changes of CH_4 and CO_2 across the catalytic bed.

The non-linear regression has been performed using Matlab routines, namely preliminary estimates were found by applying a genetic algorithm code (*ga* routine in Matlab) and optimal estimates were then obtained by applying a steepest descent method [40].

Overall, 6 parameters were optimized by fitting 112 responses obtained in 56 independent tests.

The optimized parameter estimates are listed in Table 1 alongside with 0.95 confidence intervals. The correlation matrix is reported in the SI (Table S2).

The overall fit quality can be evaluated from the parity plots in Fig. 8. All the data fall in the ± 15 % range, which proves the adequacy of the fit.

A more detailed analysis of the model adequacy is offered by the comparison between symbols and lines in Figs. 4–6.

Fig. 4 shows that by accounting for the competitive adsorption of CO in rate expressions (4) and (5), the model adequately reproduced the variable global order of the MSR (close to zero at low temperature and increasing in the range 0–1 with increasing temperature) as well as the apparent almost zeroth order of WGS, giving rise to an almost independent CO_2 production at varying CH_4 concentration.

Fig. 5, then, shows that by assuming a linear dependence of the WGS rate on H_2O partial pressure (and without any direct H_2O dependence for MSR), the enrichment of steam content in the feed was predicted to produce a positive effect on CH_4 conversion and syngas production; in fact, the promotion of rate (5) resulted in a decrease of CO concentration throughout the bed, and in turn a beneficial mitigation of CO inhibiting effect.

The data reported in Fig. 6 were especially relevant for the estimate of the CO adsorption constant; the effect by CO surface saturation on both reactions allowed to obtain a fair description of the hindering of methane conversion and of the complex evolution of syngas composition with increasing temperature; such evolution involves both the kinetic effects, prevailing in the lower temperature range, and the mass actions on the high temperature thermodynamic constraints.

3.4. Comparison between kinetic studies under concentrated and diluted conditions

On a qualitative basis, the newly proposed MSR rate expression (4) reproduces the same rate expression derived in 2008 by Donazzi et al. [26] from highly diluted kinetic experiments in annular reactor; the WGS rate expression (5) transforms instead the original zeroth order dependence on CO proposed by Pagani et al. [22] into a more

Table 1
Optimized kinetic parameters – all values are referred to catalyst pellet mass.

MSR	$k_{MSR}\ (873\ K) = 2.41\ 10^{-2} \pm 1\ 10^{-4}\ \frac{mol}{gcat\ s\ atm}$	$E_{act_{MSR}} = 101.1 \pm 6.56 kJ/mol$
WGS	$k_{WGS}\ (873\ K) = 8.11\ 10^{-2} \pm 5.5\ 10^{-3}\ \frac{mol}{gcat\ s\ atm^2}$	$E_{act_{WGS}} = 51.1 \pm 5.62\ kJ/mol$
CO adsorption	$k_{CO}\ (873\ K) = 2.11\ 10^{2} \pm 1.83\ 10^{1}\ atm^{-1}$	$\Delta H_{ads_{CO}} = -32.7 \pm 1.61\ kJ/mol$

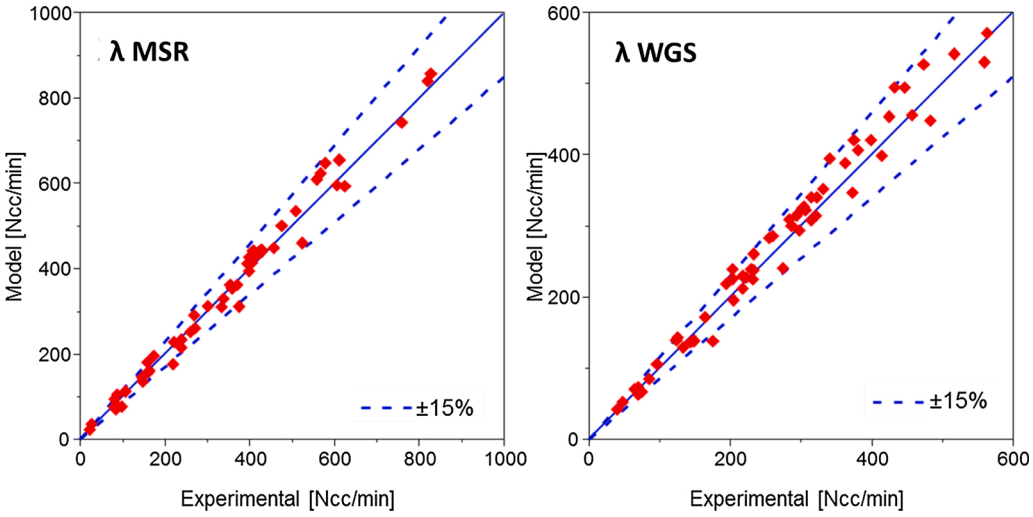

Fig. 8. Parity plots of the extent of reactions.

comprehensive and flexible form, adequate to the newly explored conditions of high reactant concentration and CO-cofeed.

A quantitative comparison between the two kinetic schemes was also performed. At this scope, Table 2 reproduces the rate expressions and estimated kinetic constants of MSR and WGS from [26] and [20], respectively. Notably, the kinetic expression of MSR in [26] has the same form of eq. (4) whereas the rate of WGS in [20] is reported in eq. 11.

$$r_{WGS}\left[20\right] = k_{WGS}\ P_{H_2O}\left(1 - K_{P,WGS}/K_{EQ,WGS}\right)\sigma_{CO}\ \left[\frac{mol}{gcat\ s}\right] \tag{11}$$

It is important to observe that the kinetic investigations in annular reactor, where the catalyst was tested in the form of an active coating deposited onto a tubular ceramic support, provided estimates of the intrinsic reaction rates for unitary washcoat mass; instead, in this work, due to the egg-shell configuration, only a portion of the catalyst is active. For the sake of comparison, we thus converted the kinetic parameters of Table 1 into those of Table 3 by referring them to the mass of active phase, which was calculated from the measurement of the egg-shell thickness.

Since the functional form of the steam reforming rate did not change, it is easily appreciated that the new set of kinetic runs, operated in a completely different experimental configuration, led to a moderate rearrangement of the parameters with a reduction of the intrinsic activity constant (k_{MSR}) at 873 K from 1.02 to 0.78 10^{-1} mol/g_{cat}/atm and an increase of the activation energy from 92 to 101 kJ/mol. Concerning the CO adsorption constant, the same value was estimated at the reference temperature of 873 K, while the estimated adsorption enthalpy passed from -37 kJ/mol in Donazzi et al. [26] to the current value of −32 kJ/mol. This partly compensated the increased temperature sensitivity of the newly proposed rate expression of MSR.

Concerning the WGS reaction, as already noted, a major formal change from the present work is represented by the introduction of an explicit dependence on CO partial pressure such that the rate expression reproduces a variable order at increasing temperature. It is interesting to note that the introduction of a temperature dependent CO-inhibition term has resulted in a lower activation energy of the revised rate expression by about 25 kJ/mol with respect to that estimated by Pagani et al. [22].

To fully appreciate the different performances of the kinetic models, two cases presented in Table 4 were simulated by assuming isothermal plug-flow reactor behavior: the first case reproduces the typical

Table 2
Kinetic parameters from Pagani et al. [22].

MSR	$k_{MSR}\ (873\ K) = 1.027\ 10^{-1}\ \frac{mol}{gcat\ s\ atm}$	$E_{act_{MSR}} = 92\ kJ/mol$
WGS	$k_{WGS}\ (873\ K) = 6.83\ 10^{-3}\ \frac{mol}{gcat\ s\ atm^2}$	$E_{act_{WGS}} = 75\ kJ/mol$
CO adsorption	$k_{CO}\ (873\ K) = 2.11\ 10^{2}\ atm^{-1}$	$\Delta H_{ads_{CO}} = -37\ kJ/mol$

Note to Table 2. Rate expression (4) for MSR, rate expression (10) for WGS.

Table 3
Kinetic parameters of this work: optimized kinetic parameters referred to active phase mass.

MSR	$k_{MSR}\ (873\ K) = 7.84\ 10^{-2}\ \frac{mol}{gcat\ s\ atm}$	$E_{act_{MSR}} = 101.1\ kJ/mol$
WGS	$k_{WGS}\ (873\ K) = 2.64\ 10^{-1}\ \frac{mol}{gcat\ s\ atm^2}$	$E_{act_{WGS}} = 51.1\ kJ/mol$
CO adsorption	$k_{CO}\ (873\ K) = 2.11\ 10^{2}\ atm^{-1}$	$\Delta H_{ads_{CO}} = -32.7\ kJ/mol$

Note to Table 3. Rate expression (4) for MSR, rate expression (5) for WGS.

Table 4
Operative conditions for comparison of representative kinetic tests performed in annular and packed foam reactor.

Cases	GHSV [Nl/h/kg_{cat}]	Feed composition		
		CH_4	H_2O	N_2
1 – Diluted conditions	$2\ 10^6$	0.01	0.025	0.965
2 – Concentrated conditions	$2\ 10^5$	0.22	0.78	0

operating conditions of the annular reactor, characterized by very high space velocity and highly diluted feed, the second case reproduces instead conditions close to the present experimental campaign in the packed foam reactor. Kinetics derived in diluted conditions (the combination of MSR rate proposed by Donazzi et al. [26] and WGS by Pagani et al. [22]) were compared with the herein presented model.

Fig. 9 shows the simulations of Case 1. Notably, under these conditions the kinetic scheme obtained from the diluted tests in annular reactor is representative of the experimental evidence, that it the true process features. Instead, the kinetic scheme obtained in this study is here significantly extrapolated and due to the larger activation energy for MSR, it tends to underestimate the extent of methane steam reforming; besides, due to the new form of WGS and the inhibiting effect of CO adsorption, the present kinetic scheme largely underestimates the extent of CO conversion into CO_2.

It must be observed, however, that the comparison between the responses of the two kinetic schemes at very high space velocity (as typical of the annular reactor) is extremely demanding.

Fig. 10 shows then the simulations of Case 2. Here, conversely, the newly proposed kinetic scheme is representative of the experimental evidence. However, the extrapolation of the kinetic scheme obtained from diluted experiments results in a large overestimation of the reaction rates, with an unrealistic full approach to equilibrium. This cannot be explained only by the moderate differences between the intrinsic rate constant and activation energy of MSR; instead, the linear dependence on H_2O and the zeroth order dependence on CO of the WGS rate expressions in [20] result in a large overestimation of the CO−CO_2 conversion route and, in turn, a strong mitigation of the inhibiting effect of CO on MSR.

In practice, the adjustment of the kinetic scheme of MSR and WGS on Rh obtained in this work involves an important moderation of the reaction rates under conditions of highly concentrated feeds. This include a significant slow-down of the WGS rate (from what would be predicted by simple extrapolation of the kinetics obtained in diluted conditions) that has a tremendous impact on the rate of MSR due to the inhibiting effect exerted by CO adsorption. It is thus concluded that extrapolation of the newly obtained kinetic scheme from concentrated to diluted feed compositions can involve some underestimation of the CO_2/CO ratio, especially at very short contact times.

4. Conclusions

The intensification of methane steam reforming is of paramount importance for the deployment of distributed H_2 production, and the use of noble-metal catalysts coupled with conductive internals is among the promising reactor solutions to overcome the heat transfer resistances and the loss of efficiency that accompany the reactor scaling-down. Moreover, the development of a small scale, isothermal reactor design offers also the opportunity to overcome the limits of the kinetic investigation, traditionally performed under diluted conditions to reduce the impact of temperature gradients across the catalytic bed and guarantee well controlled conditions.

In this work, Rh/Al_2O_3 egg-shell pellets, packed in highly conducting Cu-foams, were tested in methane steam reforming in an extensive experimental campaign that explored the use of highly concentrated feeds. The kinetic effects of methane, water, carbon monoxide and hydrogen partial pressure were investigated in the absence of radial temperature profiles. Based on the collected evidence, a refined kinetic model of MSR and WGS was proposed, which partly revisits a previously developed scheme. The new experimental campaign substantially confirmed all the prevailing kinetic dependences already identified in the past for MSR (i.e., the linear dependence on CH_4 partial pressure, the irrelevance of H_2O partial pressure and the inhibiting effect of CO) but the parameter estimates herein obtained are more robust against feed composition effects and thus suitable for the reactor design. Concerning the WGS reaction, the extension of the experimental investigation allowed to better capture the rate and kinetic dependences of the reaction, whose accurate description is of fundamental importance to correctly describe the evolutions of methane conversion and syngas composition, given the strong interplay between the two reactions.

In more general terms, we herein demonstrate how, with the adoption of conductive packed foams, it is possible to collect significant

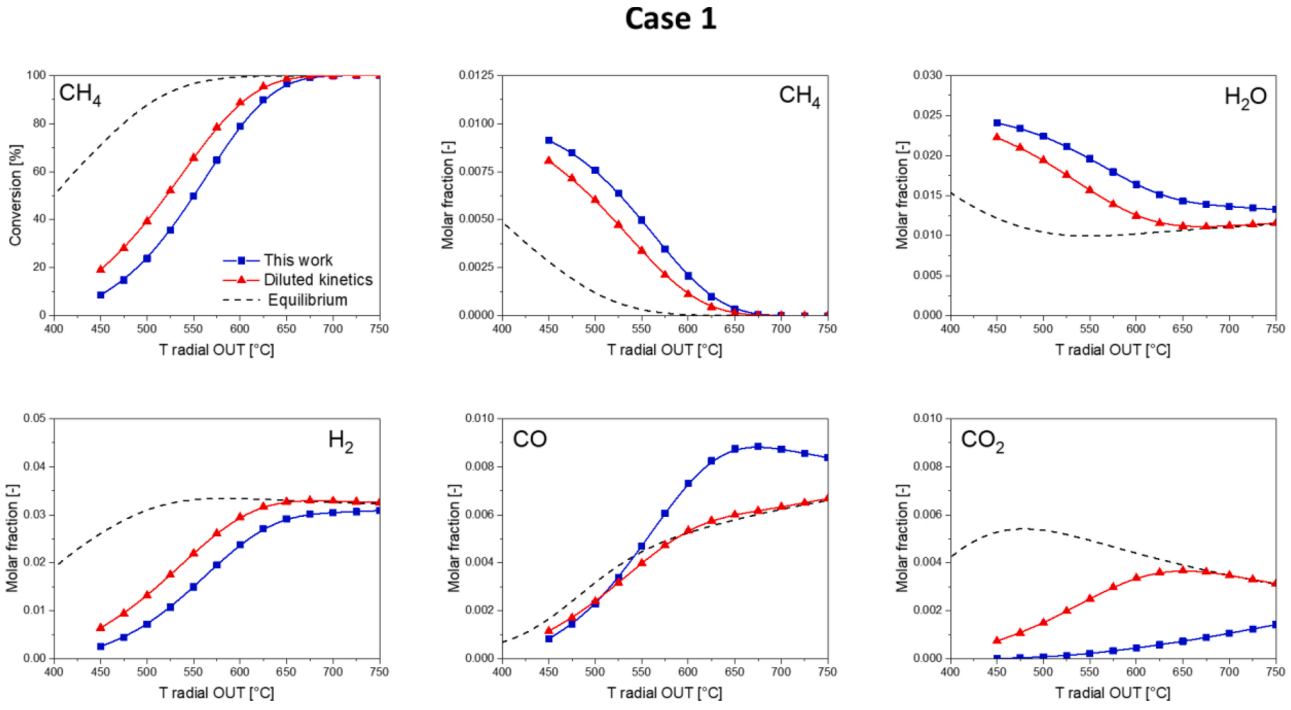

Fig. 9. Comparison of models in Case 1: (top from left) CH_4 conversion, outlet CH_4 concentration, outlet H_2O concentration, (bottom from left) outlet H_2 concentration, outlet CO concentration, outlet CO_2 concentration). Dotted lines: thermodynamic equilibrium, diluted kinetics red triangles, this work blue squares. (For interpretation of the references to colour in this figure legend, the reader is referred to the web version of this article.)

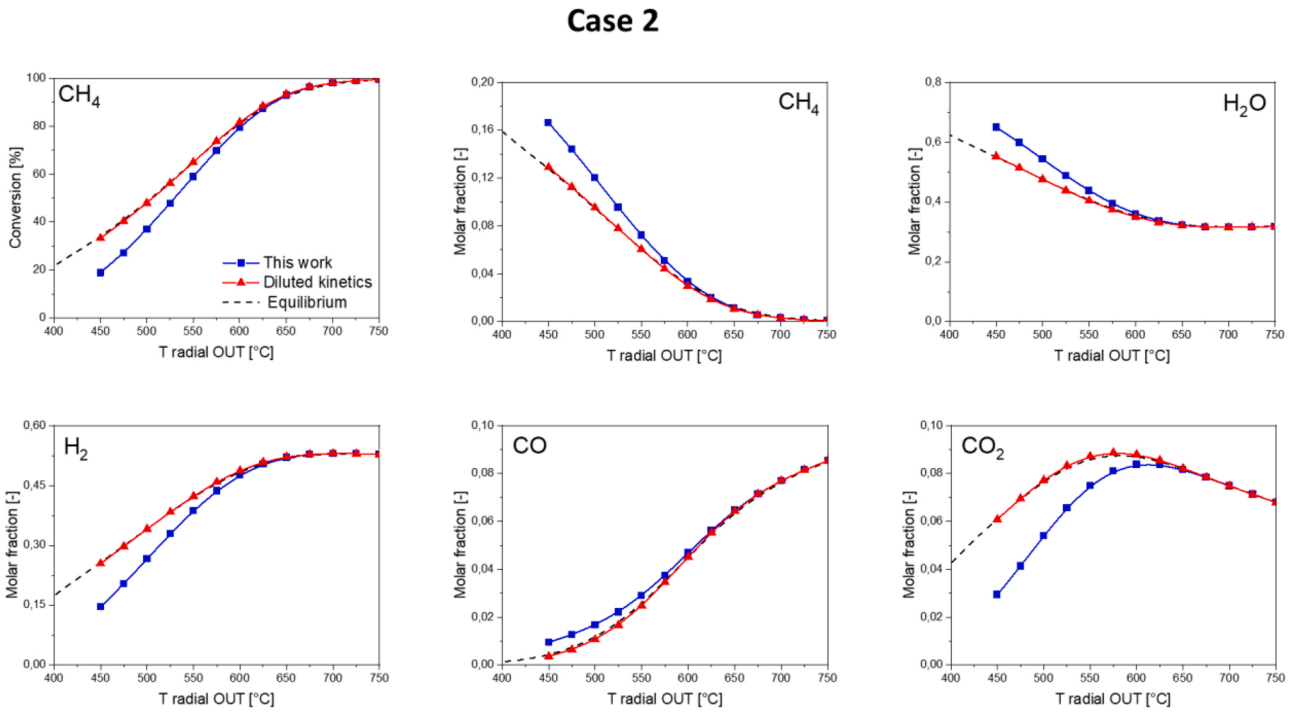

Fig. 10. Comparison of models in Case 2 : (top from left) CH_4 conversion, outlet CH_4 concentration, outlet H_2O concentration, (bottom from left) outlet H_2 concentration, outlet CO concentration, outlet CO_2 concentration). Dotted lines: thermodynamic equilibrium, diluted kinetics red triangles, this work blue squares. (For interpretation of the references to colour in this figure legend, the reader is referred to the web version of this article.)

kinetic data in realistic conditions (no dilution, high conversion) in the case of catalytic reactions with strong thermal effects. This solution can be employed for a wide set of processes, where the strong exothermicity or endothermicity of the reactions usually limits the feasibility of kinetic investigations under representative conditions.

The present study opens thus the possibility to investigate the kinetics of energy-demanding catalytic processes, reducing the uncertainties related to temperature distributions inside the catalytic bed.

CRediT authorship contribution statement

Matteo Ambrosetti: Conceptualization, Methodology, Data curation, Software, Validation, Investigation, Writing - original draft. **Danilo Bonincontro:** Conceptualization, Methodology, Data curation, Visualization, Validation, Investigation, Writing - original draft. **Riccardo Balzarotti:** Conceptualization, Methodology, Investigation, Validation. **Alessandra Beretta:** Conceptualization, Methodology, Writing - review & editing, Supervision, Project administration. **Gianpiero Groppi:** Conceptualization, Methodology, Writing - review & editing, Supervision, Project administration. **Enrico Tronconi:** Conceptualization, Methodology, Writing - review & editing, Supervision, Project administration, Funding acquisition.

Declaration of Competing Interest

The authors report no declarations of interest.

Acknowledgments

The research leading to these results has received funding from the European Research Council (ERC) under the European Union's Horizon 2020 Research and Innovation Program (Grant Agreement no. 694910/INTENT). The work of Francesco Guaresi, Massimo Capobianco and Luigi Montesano is gratefully acknowledged.

Appendix A. Supplementary data

Supplementary material related to this article can be found, in the online version, at doi:https://doi.org/10.1016/j.cattod.2021.06.003.

References

[1] https://www.iea.org/fuels-and-technologies/hydrogen, (n.d.).
[2] B. Zohuri, Hydrogen energy: challenges and solutions for a cleaner future, Hydrog. Energy Challenges Solut. a Clean. Futur. (2018) 1–283, https://doi.org/10.1007/978-3-319-93461-7.
[3] J.R. Rostrup-Nielsen, Catalysis Science and Technology Chapter 1 : Catalytic Steam Reforming, 1st editio, Springer Verlag, Berlin, Belrin, 1984.
[4] C. Murkin, J. Brightling, Eighty years of steam reforming, Johnson Matthey Technol. Rev. 60 (2016) 263–269, https://doi.org/10.1595/205651316X692923.
[5] J. Xu, G.F. Froment, Methane steam reforming, methanation and water-gas shift : 1. Intrinsic kinetics, AIChE J. 35 (1989) 88–96.
[6] E. Meloni, M. Martino, V. Palma, A short review on Ni based catalysts and related engineering issues for methane steam reforming, Catalysts. 10 (2020).
[7] Fuel Cells and Hydrogen Joint Undertaking (FCH), Hydrogen Roadmap Europe, 2019, https://doi.org/10.2843/249013.
[8] A. Beretta, G. Groppi, C. Ribani, G. Fares, C. Tregambe, Development of a catalytic fuel processor for a 10 kW combined heat and power system: experimental and modeling analysis of the steam reforming unit, ChemEngineering. 2 (2018), https://doi.org/10.3390/chemengineering2010005, 5.
[9] F. Kapteijn, J.A. Moulijn, Structured catalysts and reactors – perspectives for demanding applications, Catal. Today (2020), https://doi.org/10.1016/j.cattod.2020.09.026 in press.
[10] G. Kolb, V. Hessel, V. Cominos, H. Pennemann, J. Schürer, R. Zapf, H. Löwe, Microstructured fuel processors for fuel-cell applications, J. Mater. Eng. Perform. 15 (2006) 389–393, https://doi.org/10.1361/105994906X117161.
[11] M.A. Ashraf, S. Tacchino, N.R. Peela, G. Ercolino, K.K. Gill, D.G. Vlachos, S. Specchia, Experimental insights into the coupling of methane combustion and steam reforming in a catalytic plate reactor in transient mode, Ind. Eng. Chem. Res. 60 (2021) 196–209, https://doi.org/10.1021/acs.iecr.0c04837.
[12] G. Arzamendi, P.M. Diéguez, M. Montes, J.A. Odriozola, E.F. Sousa-Aguiar, L. M. Gandía, Methane steam reforming in a microchannel reactor for GTL intensification : a computational fluid dynamics simulation study, Chem. Eng. J. 154 (2009) 168–173, https://doi.org/10.1016/j.cej.2009.01.035.
[13] F. Minette, L. Calamote, D. Almeida, S. Ratan, J. De Wilde, Pressure drop and heat transfer of ZoneFlow TM structured catalytic reactors and reference pellets for Steam Methane reforming, Chem. Eng. J. (2020), https://doi.org/10.1016/j.cej.2020.128080, 128080.

[14] L. Sang, B. Sun, H. Tan, C. Du, Y. Wu, C. Ma, Catalytic reforming of methane with CO_2 over metal foam based monolithic catalysts, Int. J. Hydrogen Energy 37 (2012) 13037–13043, https://doi.org/10.1016/j.ijhydene.2012.05.056.
[15] F.J. Echave, O. Sanz, I. Velasco, J.A. Odriozola, M. Montes, Effect of the alloy on micro-structured reactors for methanol steam reforming, Catal. Today 213 (2013) 145–154, https://doi.org/10.1016/J.CATTOD.2013.02.027.
[16] M. Bracconi, M. Ambrosetti, M. Maestri, G. Groppi, E. Tronconi, Analysis of the effective thermal conductivity of isotropic and anisotropic Periodic Open Cellular Structures for the intensification of catalytic processes, Chem. Eng. Process. - Process Intensif. 158 (2020), https://doi.org/10.1016/j.cep.2020.108169.
[17] C.G. Visconti, E. Tronconi, G. Groppi, L. Lietti, M. Iovane, S. Rossini, R. Zennaro, Monolithic catalysts with high thermal conductivity for the Fischer-Tropsch synthesis in tubular reactors, Chem. Eng. J. 171 (2011) 1294–1307, https://doi.org/10.1016/j.cej.2011.05.014.
[18] M. Bracconi, M. Ambrosetti, M. Maestri, G. Groppi, E. Tronconi, A fundamental analysis of the influence of the geometrical properties on the effective thermal conductivity of open-cell foams, Chem. Eng. Process. - Process Intensif. 129 (2018) 181–189, https://doi.org/10.1016/j.cep.2018.04.018.
[19] P. Aghaei, C.G. Visconti, G. Groppi, E. Tronconi, Development of a heat transport model for open-cell metal foams with high cell densities, Chem. Eng. J. 321 (2017) 432–446, https://doi.org/10.1016/J.CEJ.2017.03.112.
[20] R. Balzarotti, A. Beretta, G. Groppi, E. Tronconi, A comparison between washcoated and packed copper foams for the intensification of methane steam reforming, React. Chem. Eng. 4 (2019) 1387–1392, https://doi.org/10.1039/c9re00125e.
[21] R. Balzarotti, M. Ambrosetti, A. Beretta, G. Groppi, E. Tronconi, Investigation of packed conductive foams as a novel reactor con fi guration for methane steam reforming, Chem. Eng. J. 391 (2020), https://doi.org/10.1016/j.cej.2019.123494, 123494.
[22] D. Pagani, D. Livio, A. Donazzi, A. Beretta, G. Groppi, M. Maestri, E. Tronconi, A kinetic analysis of the partial oxidation of C 3 H 8 over a 2 % Rh / Al 2 O 3 catalyst in annular microreactor, Catal. Today 197 (2012) 265–280, https://doi.org/10.1016/j.cattod.2012.09.004.
[23] G.B. Marin, S. Yablonsky, D. Constales, Kinetics of Chemical Reactions : Decoding Complexity, Wiley CH, Berlin, 2019.
[24] Y. Schuurman, Aspects of kinetic modeling of fixed bed reactors, Catal. Today 138 (2008) 15–20, https://doi.org/10.1016/j.cattod.2008.04.041.
[25] J. Wei, E. Iglesia, Isotopic and kinetic assessment of the mechanism of reactions of CH4 with CO2 or H2O to form synthesis gas and carbon on nickel catalysts, J. Catal. 224 (2004) 370–383, https://doi.org/10.1016/j.jcat.2004.02.032.
[26] J. Niu, Y. Wang, Y. Qi, A.H. Dam, H. Wang, Y. Zhu, A. Holmen, J. Ran, D. Chen, New mechanism insights into methane steam reforming on Pt / Ni from DFT and experimental kinetic study, Fuel. 266 (2020), https://doi.org/10.1016/j.fuel.2020.117143, 117143.
[27] A. Beretta, A. Donazzi, G. Groppi, P. Forzatti, V. Dal Santo, L. Sordelli, V. De Grandi, R. Psaro, Testing in annular micro-reactor and characterization of supported Rh nanoparticles for the catalytic partial oxidation of methane: effect of the preparation procedure, Appl. Catal. B Environ. 83 (2008) 96–109, https://doi.org/10.1016/J.APCATB.2008.02.007.
[28] A. Donazzi, A. Beretta, G. Groppi, P. Forzatti, Catalytic partial oxidation of methane over a 4% Rh/α-Al2O3 catalyst. Part I: Kinetic study in annular reactor, J. Catal. 255 (2008) 241–258, https://doi.org/10.1016/j.jcat.2008.02.009.
[29] A. Yamaguchi, E. Iglesia, Catalytic activation and reforming of methane on supported palladium clusters, J. Catal. 274 (2010) 52–63, https://doi.org/10.1016/j.jcat.2010.06.001.
[30] A. Donazzi, M. Maestri, B.C. Michael, A. Beretta, P. Forzatti, G. Groppi, E. Tronconi, L.D. Schmidt, D.G. Vlachos, Microkinetic modeling of spatially resolved autothermal CH4 catalytic partial oxidation experiments over Rh-coated foams, J. Catal. 275 (2010) 270–279, https://doi.org/10.1016/j.jcat.2010.08.007.
[31] R.B.S. Junior, A. Beretta, A. Mostafa, G. Groppi, Catalytic partial oxidation of ethanol over Rh-coated monoliths investigated by the axially resolved sampling technique : effect of H2O, Catal. Today (2020), https://doi.org/10.1016/j.cattod.2020.09.030.
[32] A. Carrera, M. Pelucchi, A. Stagni, A. Beretta, G. Groppi, ScienceDirect Catalytic partial oxidation of n-octane and iso- octane : experimental and modeling results, Int. J. Hydrogen Energy 42 (2017) 24675–24688, https://doi.org/10.1016/j.ijhydene.2017.08.020.
[33] A. Porta, L. Falbo, C.G. Visconti, L. Lietti, C. Bassano, P. Deiana, Synthesis of Ru-based catalysts for CO_2 methanation and experimental assessment of intraporous transport limitations, Catal. Today (2019), https://doi.org/10.1016/J.CATTOD.2019.01.042.
[34] M. Ambrosetti, M. Bracconi, M. Maestri, G. Groppi, E. Tronconi, Packed foams for the intensification of catalytic processes: assessment of packing efficiency and pressure drop using a combined experimental and numerical approach, Chem. Eng. J. 382 (2020), https://doi.org/10.1016/j.cej.2019.122801, 122801.
[35] J.L. Silveira, Sustainable Hydrogen Production Process, Springer, New York, 2017.
[36] M. Maestri, D.G. Vlachos, A. Beretta, G. Groppi, E. Tronconi, Steam and dry reforming of methane on Rh : microkinetic analysis and hierarchy of kinetic models, J. Catal. 259 (2008) 211–222, https://doi.org/10.1016/j.jcat.2008.08.008.
[37] B.T. Schadel, M. Duisberg, O. Deutschmann, Steam reforming of methane, ethane, propane, butane, and natural gas over a rhodium-based catalyst, Catal. Today 142 (2009) 42–51, https://doi.org/10.1016/j.cattod.2009.01.008.
[38] C. Karakaya, R. Otterstätter, L. Maier, O. Deutschmann, Kinetics of the water-gas shift reaction over Rh / Al 2 O 3 catalysts, Applied Catal. A, Gen. 470 (2014) 31–44, https://doi.org/10.1016/j.apcata.2013.10.030.
[39] M. Maestri, D.G. Vlachos, A. Beretta, P. Forzatti, G. Groppi, E. Tronconi, Dominant Reaction Pathways in the Catalytic Partial Oxidation of CH 4 on Rh, Top. Catal. 52 (2009) 1983–1988, https://doi.org/10.1007/s11244-009-9374-2.
[40] J.S. Arora, Introduction to Optimum Design, second edition, Academic Press, Cambridge, 2004.